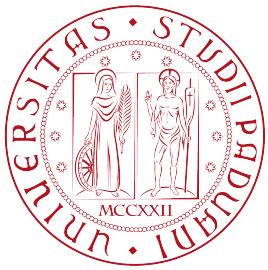

UNIVERSITY OF PADOVA

MASTER DEGREE IN PHYSICS

REPORTS FOR PHYSICS LABORATORY EXPERIMENTS

Author:
Luca Teodori
Student 1179540

Experiments:
1. Environmental radiation
2. Compton scattering
3. Digital Imaging

Academic Year 2017/2018

Contents

1 Measurement of Environmental Radiation with Gamma Spectroscopy Techniques

The objectives of the experiment are:

1. To measure environmental radioactivity in the samples of different organic or inorganic materials;
2. To perform an "indoor" radon measurement for a room of the Polo didattico building.

The experimental apparatus consists of a shielded well equipped with two detectors for gamma spectroscopy: a NaI(Tl) scintillation detector and a HPGe detector (hyper-pure germanium detector) operated at the liquid nitrogen temperature.

1.1 Experiment and data analysis

1.1.1 Calibration

In figures 1.1 - 1.5 we show the source spectra of the calibration procedure of the two detectors and in table 1.2 we resume the calibration procedure.

In figure 1.6 we show the calibration line we obtained whereas in table 1.1 we resume the computation of the resolutions of the detectors (we recall that the following, for a gaussian, holds: $\mathrm{FWHM} = 2\sqrt{2\ln 2}\,\sigma$).

To measure the intrinsic efficiency of the full energy peak of a detector, i.e. the ratio between the number of events in that peak divided by the number of photons that hit the detector, we must subtract the background (normalized with the time of acquisition of the various source spectra) from the spectra we obtained; to determine the number of photons N_γ that hit the detector we can use the following:

$$N_\gamma = \frac{\text{N of decays}}{\text{seconds}} \times t \times \frac{\text{N of } \gamma \text{ of transition}}{\text{N of decays}} \times \frac{\Omega}{4\pi}\ , \tag{1}$$

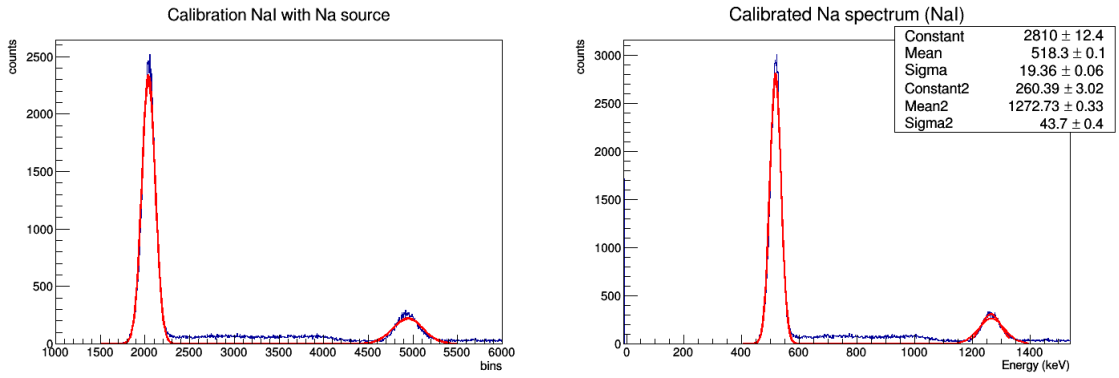

Figure 1.1: ^{22}Na source spectrum for the two peaks for calibration of the NaI detector.

Peak (keV) & distance NaI	Resolution
59 (20 cm)	0.20
511 (3 cm)	0.09
1275 (3 cm)	0.08
HPGe	
59 (23 cm)	0.024
511 (7 cm)	0.006
511 (23 cm)	0.006
1275 (7 cm)	0.002
1275 (23 cm)	0.002

Table 1.1: Resume of the resolutions of the detectors, in the first column are indicated also the distances from the relative detector. Notice that the resolution for the HPGe differs with respect to the one for the NaI for almost an order of magnitude. Notice also that we obtained a much worse resolution for the low energy corresponding to the americium peak.

Detector	energy calibration (keV)	
	m	q
HPGe	0.13404 ± 0.0001	-6.153 ± 0.573
NaI	0.2584 ± 0.0058	-9.54 ± 5.47

Table 1.2: Resume of the calibration of the detectors.

Source	Activity measured (kBq)	Half life (years)	Activity (experiment) (kBq)
^{22}Na	2.2	2.60	1.62
^{241}Am	380	432.2	379.3
^{152}Eu	102.5	13.52	96.65

Table 1.3: Values of the various activities used for the intrinsic efficiency measure of the detectors; values of the activity of the source are taken by `http://www.dfa.unipd.it/fileadmin/servtec/Sorgenti_polo_sett_2016.pdf`; the activity measured refer to September 2016 whereas the activities at the date of the experiment refer to November 2017, and are computed using the half life of the isotope.

where Ω is the solid angle of the detector viewed by the source and t the time of acquisition; to calculate Ω we treated the source as a point source and used the relation that relates the angular opening of a cone α with the corresponding solid angle, i.e.

$$\Omega = 2\pi\left(1 - \cos\frac{\alpha}{2}\right) , \tag{2}$$

whereas for α we used $\frac{\alpha}{2} = \arctan\frac{h}{d}$, where d is the distance source-detector and h is the radius of the basis of the cone, obtained from the area of the detectors (1200 mm^2 for the HPGe and 17670 mm^2 for the NaI). The results are resumed in table 1.5, and we remark that there and in the following the errors on counts are taken to be the square root of the counts, the errors on distances are taken to be 0.2 cm (they were measured with a ruler) whereas the errors on the derived quantities are obtained with propagation.

We also performed the measurement of the relative efficiency curve of the HPGe with a ^{152}Eu source. Figure 1.7 shows the ^{152}Eu spectrum with subtracted background and the plot of relative efficiencies versus the various peaks of the source. We normalized the areas of the peaks in order to have a nominal value of 100 for the transition to 1408 keV. In the peak analysis we omitted the ones at 1085 and 1089 because they are too close to each other to be distinguished.

We notice by looking at table 1.6 that the behavior of relative efficiencies with the energy is highly irregular, this is probably due to the great uncertainties in the integrals

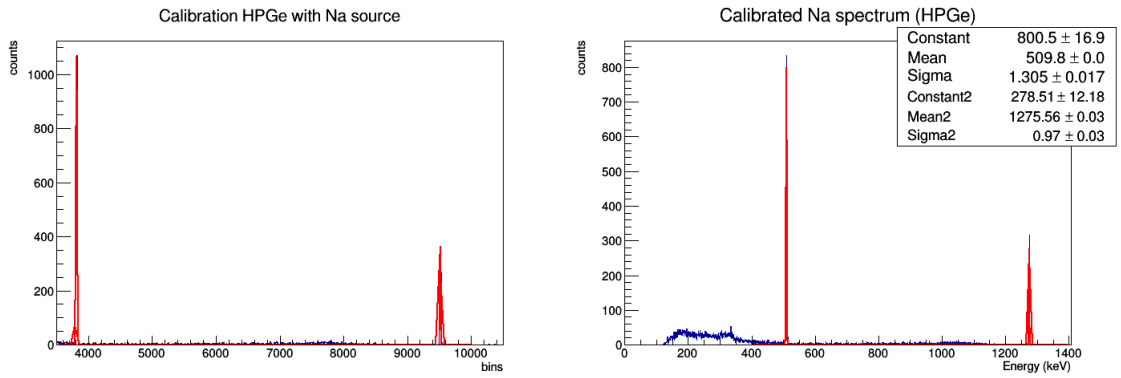

Figure 1.2: ^{22}Na source spectrum for the two peaks for calibration of the HPGe detector.

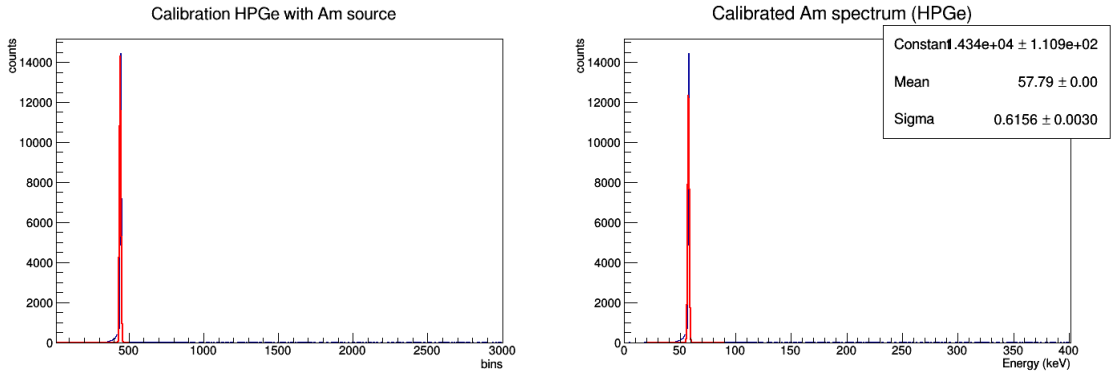

Figure 1.3: ^{141}Am source spectrum of the peak for calibration.

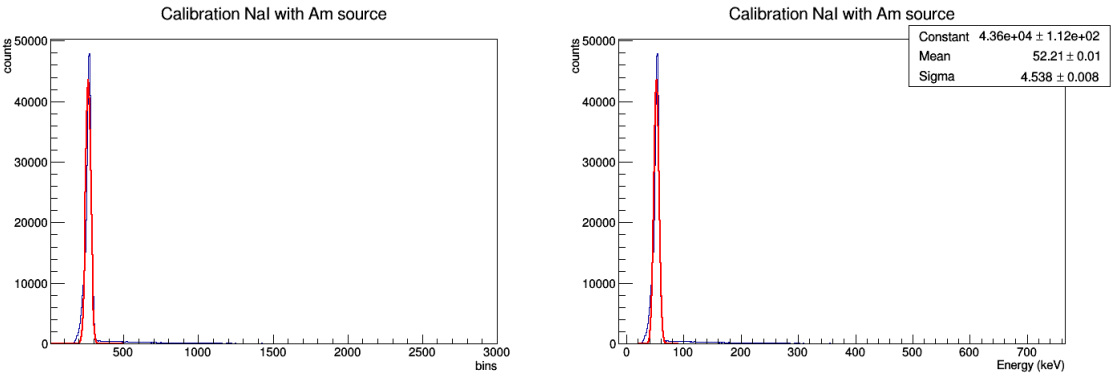

Figure 1.4: ^{141}Am source spectrum of the peak for calibration at 20 cm distance from the NaI detector.

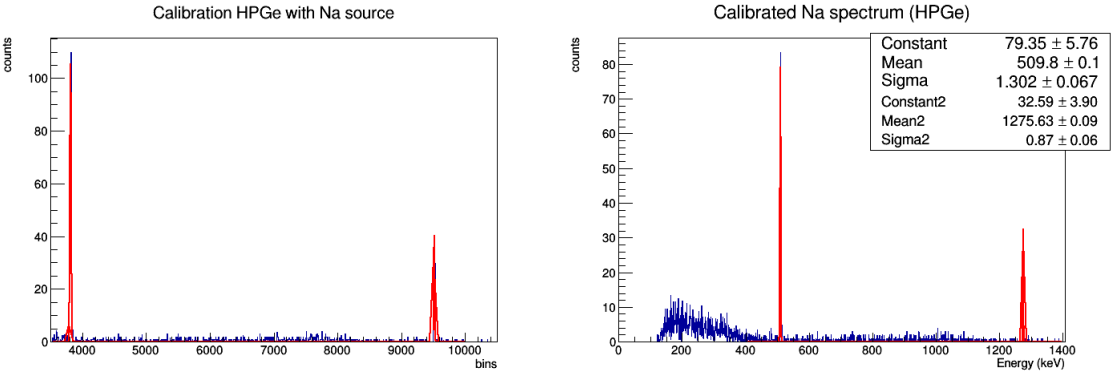

Figure 1.5: ^{22}Na source spectrum for the two peaks for calibration of the HPGe at 23 cm distance from it.

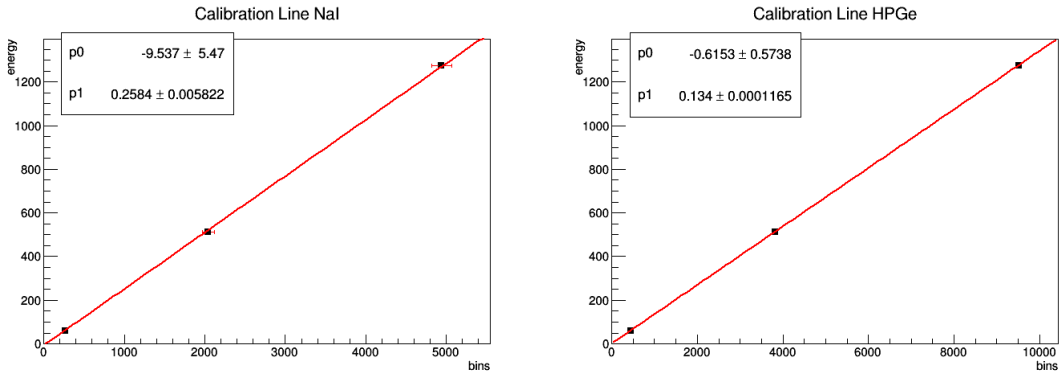

Figure 1.6: Calibration lines obtained with the peak for the ^{141}Am and the two peaks of the ^{22}Na .

Type of peak	Activity (kBq)	time (s)	f	Ω (NaI)	Ω (HPGe)
Am (23cm)	379.3	359	0.36	-	0.022 ± 0.001
Na(511)(3cm)	1.62	285	1.8	2.36 ± 0.04	0.231 ± 0.003
Na(1275)(3cm)	1.62	285	1	2.36 ± 0.04	0.2303 ± 0.003
Am (20cm)	379.3	600	0.36	0.107 ± 0.002	-
Na(511)(23cm)	1.62	172	1.8	-	0.022 ± 0.001
Na(1275)(23cm)	1.62	172	1	-	0.022 ± 0.001

Table 1.4: Values of the various parameters used for the intrinsic efficiency measure of the detectors; the 3 cm and 20 cm ones are the distances from the NaI, whereas the other are the distances from the HPGe; here f is the fraction yields by the gamma transition; the solid angle values that are not reported refer to situations where the source was not aligned with that detector.

Type of peak	N of events	Intrinsic efficiency
	NaI detector	
Na1	155950 ± 5274	0.571 ± 0.034
Na2	86639 ± 2930	0.208 ± 0.034
Am	701076 ± 6803	0.502 ± 0.010
	HPGe detector	
Type of peak	N of events	Intrinsic efficiency
Am	87550 ± 757	0.324 ± 0.009
Na1	9031 ± 190	0.250 ± 0.027
Na2	5017 ± 105	0.117 ± 0.027
Na1(23)	896 ± 8	0.260 ± 0.012
Na2(23)	498 ± 4	0.127 ± 0.010

Table 1.5: Intrinsic efficiency measure of the detectors.

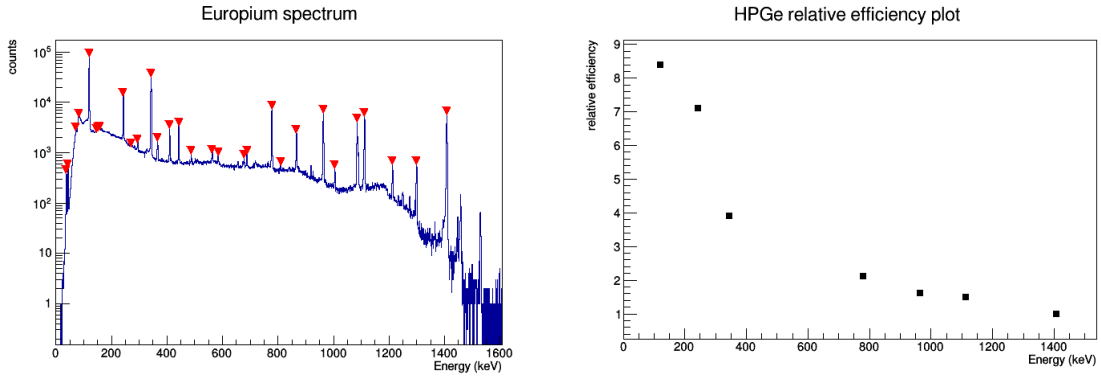

Figure 1.7: On the left, ^{152}Eu spectrum with subtracted background; on the right, the plot of relative efficiency versus the various peaks of the ^{152}Eu source (only the values relative to the peaks with enough statistic are included).

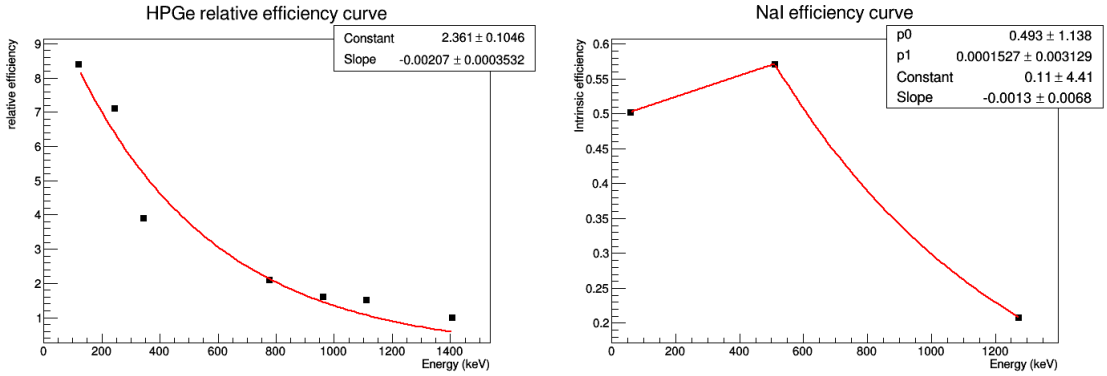

Figure 1.8: Relative efficiency curve for the detectors. As a fitting function we used an exponential for the HPGe and an order 1 polynome plus an exponential for the NaI. Notice that we obtained relative high efficiencies for the NaI detector, and the conversion to the intrinsic efficiency for the HPGe will result in high values too; this could be the reason of some discrepancies regarding the activity measures.

of the peaks with not enough statistic and the difficulty to isolate in the histogram the events that are only due to the peak under exam (the reported errors on these measures are given by the square root of the number of events, but this is surely an underestimation). In order to obtain a more reliable efficiency curve (showed in figure 1.7), we have restricted the analysis only to the peaks that have a normalized number of events of 90 or more.

1.1.2 Sample analysis

The second session of the experiment consisted on the determination of some sample activities. We used a sample of pellet and a sample of plaster. To determine the presence of a given radionuclide in a sample, we analyzed the peaks of the two spectra (with subtracted background) and compare their energy with the typical energy peaks

Peak (keV)	N of events (normalized)	Relative efficiency
121.8	1190 ± 2.2	8.44 ± 0.13
244.7	260 ± 1.0	7.10 ± 0.20
344.3	500 ± 1.4	3.93 ± 0.04
367.5	48 ± 0.4	11.46 ± 1.20
411.1	70 ± 0.5	6.54 ± 0.32
444.0	70 ± 0.5	4.67 ± 0.16
488.7	34 ± 0.4	17.14 ± 3.18
586.3	45 ± 0.4	20.09 ± 3.80
678.6	45 ± 0.4	19.60 ± 3.62
688.7	42 ± 0.4	10.19 ± 1.01
778.9	132 ± 0.7	2.11 ± 0.03
867.4	58 ± 0.5	2.82 ± 0.07
964.0	113 ± 0.7	1.61 ± 0.02
1005.1	16 ± 0.3	4.48 ± 0.32
1112.1	97 ± 0.6	1.49 ± 0.02
1212.9	15 ± 0.2	2.25 ± 0.08
1299.1	11 ± 0.2	1.42 ± 0.04
1408.0	100 ± 0.6	1.00 ± 0.01

Table 1.6: Relative efficiency measure of the HPGe for the europium peaks.

of the various radionuclide[1]. Another goal of this part of the experiment is the measure of the activity of the sources. In order to do this, we need the number of photons emitted by the source corresponding to each peak. The formula we applied to estimate the number of photons N_γ corresponding to each peak is:

$$N_\gamma = \frac{\text{N of counts}}{\text{Absolute efficiency}} \ .$$

Then the overall activity of the sample is obtained by summing all the relative activities, where the relative activities are obtained with

$$A = \frac{N_\gamma}{t}\frac{4\pi}{\Omega} \ ,$$

where one takes into account the portion of solid angle covered by the detector (we assumed an isotropic emission for the sources). From the calibration part, for the NaI detector we only know the absolute efficiencies at the energies 59, 511 and 1275 keV; in order to obtain the other absolute efficiencies we interpolated them , whereas for the HPGe detector we obtained the relative curve efficiency (see figure 1.8), and in order to obtain the new absolute efficiencies we used the intrinsic efficiency obtained for the HPGe at 511 keV energy (showed in table 1.5) to obtain the conversion factor.

The spectral analysis for the pellet sample is resumed in figure 1.9 and in table 1.7, whereas the spectral analysis for the plaster is resumed in figure 1.10 and in table 1.8.

[1] All the identifications of the peaks with the corresponding radionuclide refer to the data in `http://www.cpp.edu/~pbsiegel/bio431/genergies.html`.

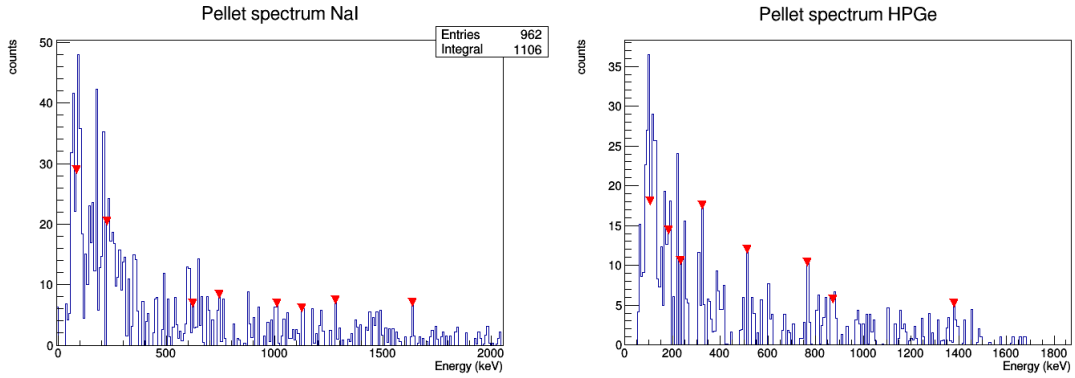

Figure 1.9: Source spectrum of pellet and relative peaks

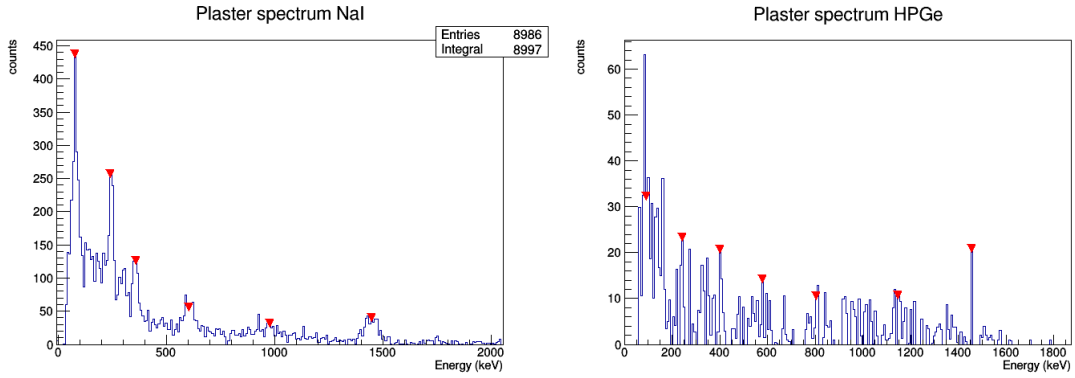

Figure 1.10: Source spectrum of plaster and relative peaks.

In all of these kind of tables, we showed also the percent that a transitions yields in terms of the activity, showed in the "percent" column.

We notice that the activities measured are constantly higher for the HPGe detector, and this is an issue that is present also on the radon counting measurements illustrated on the next section.

1.1.3 Radon counting

In this last part of the experiment we describe our measure procedure for the radon measurement for a room of the Polo didattico building. We placed a canister at the chosen room and retrieved it after 24 hours. So we measured the spectra of the exposed canister, a non exposed canister for the background measure and a calibrated canister with known activity.

In figures 1.11-1.13 and in tables 1.9-1.11 are resumed the results of the three canisters analysis.

Thanks to the data acquired, we can measure the radon activity per liter of air RN with

$$\mathrm{RN} = \frac{N}{\mathrm{DF} \times E \times \mathrm{CF} \times t} \ ,$$

Pellet analysis
Measurement time: 740 s
Weight: 0.194 kg

NaI detector					
Peak (keV)	Counts	Efficiency	Activity (Bq/kg)	Percent	Radionuclide
85	272 ± 16	0.506 ± 0.020	20.01 ± 1.21	0.23	^{155}Eu
225	456 ± 21	0.527 ± 0.021	32.19 ± 1.51	0.38	^{212}Pb
621	131 ± 11	0.494 ± 0.020	9.88 ± 0.86	0.12	^{126}Ru
745	45 ± 6	0.419 ± 0.017	4.00 ± 0.60	0.05	^{92}Nb
1009	40 ± 6	0.296 ± 0.012	5.04 ± 0.80	0.06	^{101}Mo
1125	31 ± 5	0.254 ± 0.010	4.55 ± 0.82	0.05	^{214}Bi
1280	23 ± 4	0.207 ± 0.008	4.14 ± 0.86	0.05	^{24}Na
1636	20 ± 4	0.129 ± 0.005	5.77 ± 1.29	0.07	^{38}Cl
Total activity with NaI: 85.58 ± 7.95 Bq/kg					
HPGe detector					
Peak (keV)	Counts	Efficiency	Activity (Bq/kg)	Percent	Radionuclide
108	237 ± 15	0.576 ± 0.069	156.63 ± 10.18	0.16	^{155}Eu
180	129 ± 11	0.496 ± 0.060	98.95 ± 8.71	0.10	^{226}Ra
235	67 ± 8	0.443 ± 0.053	57.59 ± 7.04	0.06	^{212}Pb
325	89 ± 9	0.367 ± 0.044	92.16 ± 9.77	0.09	^{125}Sn
512	55 ± 7	0.249 ± 0.030	83.87 ± 11.31	0.08	^{22}Na
767	40 ± 6	0.147 ± 0.018	103.39 ± 16.35	0.10	^{92}Nb
870	38 ± 6	0.119 ± 0.014	121.56 ± 19.72	0.12	^{160}Tb
1380	30 ± 5	0.041 ± 0.005	275.75 ± 50.35	0.28	^{24}Na
Total activity with HPGe: 989.91 ± 133.42 Bq/kg					

Table 1.7: Data elaboration for the measure of the activity of the pellet sample.

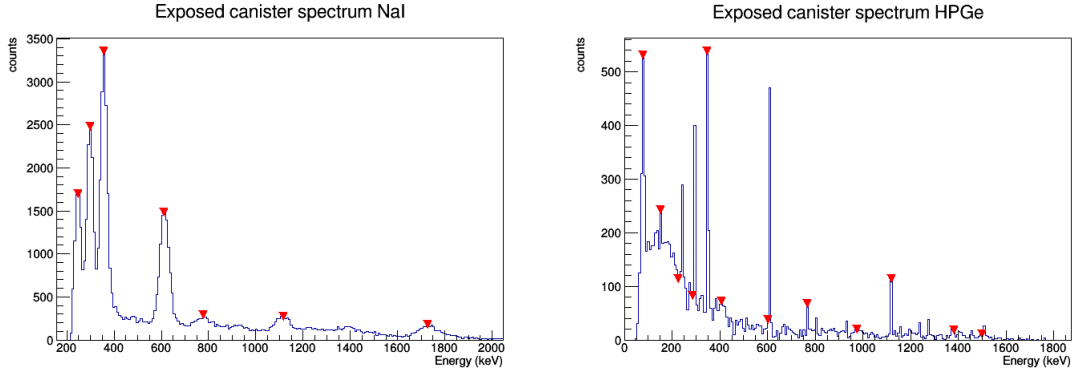

Figure 1.11: Source spectrum of the exposed canister and relative peaks.

Plaster analysis
Measurement time: 1130 s
Weight: 0.322 kg

NaI detector					
Peak (keV)	Counts	Efficiency	Activity (Bq/kg)	Percent	Radionuclide
77	2980 ± 54	0.505 ± 0.020	86.72 ± 1.59	0.30	^{234}Th
242	2578 ± 50	0.530 ± 0.021	71.46 ± 1.41	0.25	^{212}Pb
357	1100 ± 33	0.547 ± 0.022	29.51 ± 0.89	0.10	^{211}Pb
605	926 ± 30	0.504 ± 0.020	26.97 ± 0.89	0.09	^{208}Tl
976	715 ± 26	0.309 ± 0.012	34.01 ± 1.27	0.12	^{160}Tb
1446	481 ± 21	0.166 ± 0.007	42.58 ± 1.94	0.15	^{40}K

Total activity with NaI: 291.26 ± 7.99 Bq/kg

HPGe detector					
Peak (keV)	Counts	Efficiency	Activity (Bq/kg)	Percent	Radionuclide
93	409 ± 20	0.594 ± 0.071	103.39 ± 5.11	0.10	^{234}Th
242	121 ± 11	0.436 ± 0.053	41.63 ± 3.79	0.04	^{212}Pb
400	146 ± 12	0.315 ± 0.038	69.67 ± 5.77	0.07	^{211}Pb
580	145 ± 12	0.217 ± 0.026	100.42 ± 8.34	0.10	^{208}Tl
805	76 ± 8	0.136 ± 0.016	83.85 ± 9.62	0.08	^{58}Co
1149	98 ± 9	0.067 ± 0.008	220.34 ± 22.26	0.22	^{135}I
1456	88 ± 9	0.035 ± 0.004	373.49 ± 39.82	0.38	^{40}K

Total activity with HPGe: 992.79 ± 94.70 Bq/kg

Table 1.8: Data elaboration for the measure of the activity of the plaster sample.

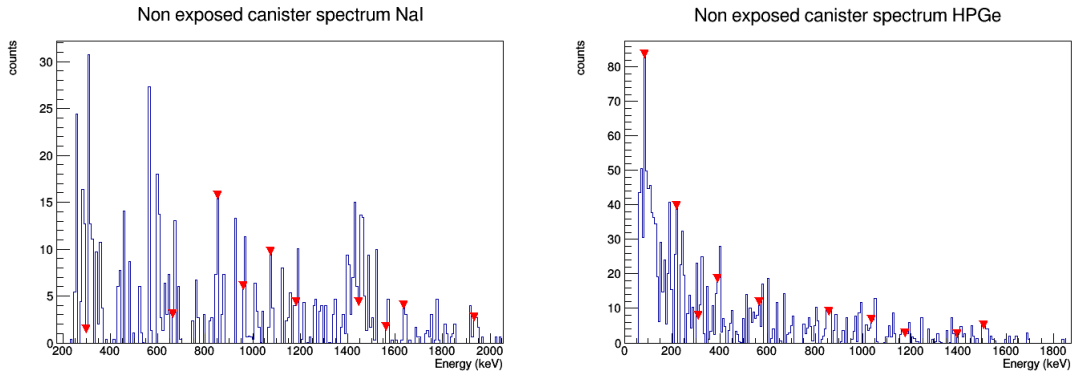

Figure 1.12: Source spectrum of the non exposed canister and relative peaks.

Exposed canister analysis
Measurement time: 1200 s
Weight: 0.159 kg

NaI detector

Peak (keV)	Counts	Efficiency	Activity (Bq/kg)	Percent	Radionuclide
250	8266 ± 90	0.531 ± 0.021	435.93 ± 4.82	0.10	^{212}Pb
300	12070 ± 109	0.539 ± 0.022	627.53 ± 5.75	0.15	^{214}Pb
357	17650 ± 132	0.547 ± 0.022	903.05 ± 6.86	0.21	^{214}Pb
613	13840 ± 117	0.499 ± 0.020	776.96 ± 6.65	0.18	^{214}Bi
778	4876 ± 69	0.401 ± 0.016	340.44 ± 4.89	0.08	^{131}I
1116	4400 ± 66	0.257 ± 0.010	480.24 ± 7.26	0.11	^{214}Bi
1727	2926 ± 54	0.114 ± 0.005	716.18 ± 13.26	0.17	^{214}Bi

Total activity with NaI: 4280.33 ± 49.49 Bq/kg

HPGe detector

Peak (keV)	Counts	Efficiency	Activity (Bq/kg)	Percent	Radionuclide
79	1820 ± 42	0.611 ± 0.074	852.31 ± 20.00	0.07	^{44}Ti
152	2394 ± 48	0.525 ± 0.063	1303.95 ± 26.68	0.10	^{141}Ce
240	1389 ± 37	0.438 ± 0.053	907.68 ± 24.37	0.07	^{212}Pb
288	1113 ± 33	0.397 ± 0.048	803.28 ± 24.09	0.06	^{214}Pb
348	1412 ± 37	0.350 ± 0.042	1153.81 ± 30.73	0.09	^{214}Pb
407	902 ± 30	0.310 ± 0.037	832.78 ± 27.74	0.06	^{211}Pb
602	1150 ± 33	0.207 ± 0.025	1589.60 ± 46.90	0.12	^{214}Bi
767	396 ± 19	0.147 ± 0.018	770.16 ± 38.71	0.06	^{131}I
977	295 ± 17	0.095 ± 0.011	886.05 ± 51.60	0.07	^{115}Cd
1120	404 ± 20	0.071 ± 0.009	1631.33 ± 81.18	0.13	^{214}Pb
1381	129 ± 11	0.041 ± 0.005	893.99 ± 78.72	0.07	^{24}Na
1500	143 ± 12	0.032 ± 0.004	1267.75 ± 106.02	0.10	^{42}K

Total activity with HPGe: 12892.68 ± 556.75 Bq/kg

Table 1.9: Data elaboration for the measure of the activity of the exposed canister. The peaks in red are the ones belonging to the radon chain.

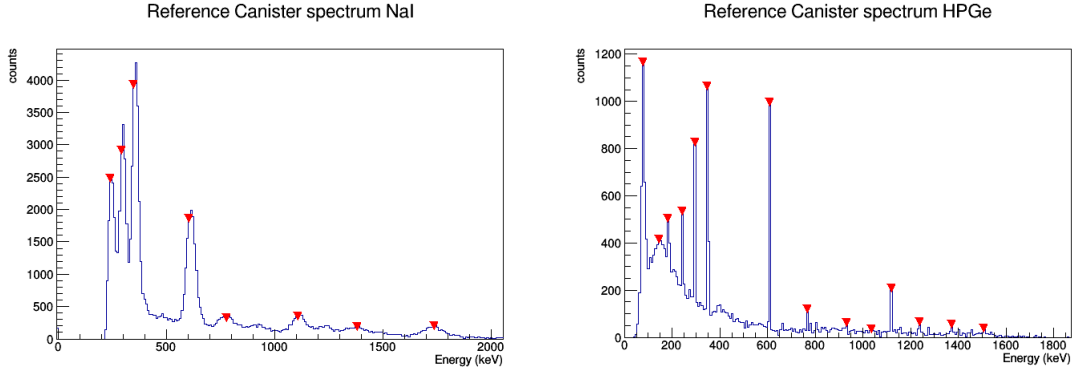

Figure 1.13: Source spectrum of the reference canister and relative peaks.

Non exposed canister analysis
Measurement time: 1180 s
Weight: 0.155 kg

NaI detector

Peak (keV)	Counts	Efficiency	Activity (Bq/kg)	Percent	Radionuclide
300	146 ± 12	0.539 ± 0.022	7.92 ± 0.66	0.11	^{171}Er
580	148 ± 12	0.521 ± 0.021	8.30 ± 0.68	0.12	^{207}Bi
853	53 ± 7	0.363 ± 0.015	4.26 ± 0.59	0.06	^{131}Te
960	48 ± 6	0.315 ± 0.013	4.45 ± 0.64	0.06	^{160}Tb
1075	32 ± 5	0.271 ± 0.011	3.45 ± 0.61	0.05	^{131}Te
1183	69 ± 8	0.235 ± 0.009	8.58 ± 1.03	0.12	^{60}Co
1447	124 ± 11	0.166 ± 0.007	21.87 ± 1.96	0.32	^{40}K
1910	31 ± 5	0.090 ± 0.004	10.08 ± 1.81	0.15	^{56}Mn

Total activity with NaI: 68.91 ± 7.98 Bq/kg

HPGe detector

Peak (keV)	Counts	Efficiency	Activity (Bq/kg)	Percent	Radionuclide
86	550 ± 23	0.602 ± 0.073	272.61 ± 11.63	0.12	^{155}Eu
220	270 ± 16	0.456 ± 0.055	176.60 ± 10.75	0.08	^{97}Ru
310	143 ± 12	0.379 ± 0.046	112.68 ± 9.42	0.05	^{171}Er
392	134 ± 11	0.320 ± 0.038	125.12 ± 10.81	0.06	^{113}Sn
565	166 ± 12	0.224 ± 0.027	221.72 ± 17.21	0.10	^{207}Bi
856	105 ± 10	0.122 ± 0.015	256.11 ± 25.00	0.11	^{131}Te
1036	101 ± 10	0.084 ± 0.010	357.56 ± 35.58	0.16	^{131}Te
1182	43 ± 6	0.062 ± 0.008	205.93 ± 31.40	0.09	^{60}Co
1396	33 ± 5	0.040 ± 0.005	246.10 ± 42.84	0.11	^{152}Eu
1508	31 ± 5	0.032 ± 0.004	291.48 ± 52.35	0.13	^{42}K

Total activity with HPGe: 2265.91 ± 246.99 Bq/kg

Table 1.10: Data elaboration for the measure of the activity of the non exposed canister.

Reference canister analysis
Measurement time: 1185 s
Weight: 0.170 kg

NaI detector					
Peak (keV)	Counts	Efficiency	Activity (Bq/kg)	Percent	Radionuclide
241	12310 ± 111	0.530 ± 0.021	616.47 ± 5.59	0.11	^{212}Pb
291	15280 ± 123	0.537 ± 0.021	754.34 ± 6.15	0.13	^{214}Pb
349	23160 ± 152	0.546 ± 0.022	1124.83 ± 7.48	0.20	^{214}Pb
605	17330 ± 131	0.504 ± 0.020	911.75 ± 6.99	0.16	^{214}Bi
778	5465 ± 73	0.401 ± 0.016	361.39 ± 4.90	0.06	^{131}I
1108	5200 ± 72	0.259 ± 0.010	531.90 ± 7.40	0.09	^{214}Bi
1380	4140 ± 64	0.181 ± 0.007	606.69 ± 9.45	0.11	^{24}Na
1735	3340 ± 57	0.113 ± 0.005	782.53 ± 13.56	0.14	^{214}Bi

Total activity with NaI: 5689.90 ± 61.53 Bq/kg

HPGe detector					
Peak (keV)	Counts	Efficiency	Activity (Bq/kg)	Percent	Radionuclide
78	4081 ± 63	0.612 ± 0.074	1806.36 ± 28.34	0.08	^{44}Ti
145	3703 ± 60	0.533 ± 0.064	1882.82 ± 31.00	0.08	^{141}Ce
183	3158 ± 56	0.493 ± 0.059	1737.08 ± 30.96	0.07	^{226}Ra
243	1545 ± 39	0.435 ± 0.052	962.20 ± 24.50	0.04	^{212}Pb
295	1844 ± 42	0.391 ± 0.047	1278.89 ± 29.81	0.05	^{214}Pb
347	2394 ± 48	0.351 ± 0.042	1848.99 ± 37.84	0.08	^{214}Pb
609	2044 ± 45	0.204 ± 0.025	2715.02 ± 60.12	0.11	^{214}Bi
767	670 ± 25	0.147 ± 0.018	1234.17 ± 47.70	0.05	^{131}I
931	450 ± 21	0.105 ± 0.013	1163.89 ± 54.88	0.05	^{115}Cd
1036	344 ± 18	0.084 ± 0.010	1105.69 ± 59.63	0.05	^{207}Bi
1119	539 ± 23	0.071 ± 0.009	2057.13 ± 88.63	0.09	^{214}Bi
1238	355 ± 18	0.056 ± 0.007	1733.23 ± 92.01	0.07	^{91}Y
1373	308 ± 17	0.042 ± 0.005	1988.45 ± 113.32	0.08	^{24}Na
1508	279 ± 16	0.032 ± 0.004	2381.79 ± 142.62	0.10	^{42}K

Total activity with HPGe: 23895.71 ± 841.34 Bq/kg

Table 1.11: Data elaboration for the measure of the activity of the reference canister. The peaks in red are the ones belonging to the radon chain.

where t is the time of exposure in minutes (in our case $t = 1440$ min); DF is the decay factor that takes into account that some of the radon can decay before being counted, and it is

$$\mathrm{DF} = e^{-\frac{0.693t}{5501}} \ ,$$

where t is the time in minutes from the exposure period of the canister to when its activity is measured (since in our experiment t is of the order of 10 minutes, this factor is almost negligible); E is the net number of counts per a certain unit of time per Bq for the reference canister, and it is a factor that allows us to convert the number of counts in activity without passing through the efficiencies calculations and all the stuff we have previously done for the measures of the activities; N is the corresponding net number of counts in the exposed canister (background subtracted, with the same unit of time used for the measure of E in the reference canister); CF is the calibration factor. To obtain the calibration factor, we need the so called water gain, i.e. the increase in weight due to absorption of water vapor. Since our measured water gain (for a 24 hours exposure) is greater than 4 g (it is 4.2 g), we can establish that the average humidity during the exposure was 80 %. Using the plots for CF and for AF (moisture dependent adjustment factor) given in the notes for the experiment, we calculated a CF=0.12 L/min.

For the measure of N and E, we must recognize first a region of interest for the analysis corresponding to the most important gamma transitions relative to radon, and we recognize the peaks belonging to the radon chain by writing them in red in table 1.11 and in table 1.9. Then we know the activity of the reference canister ($A =$ 3.05 kBq/kg), and with all this we computed $N = 42.44 \pm 0.28$ events/s and $E = 0.10 \pm 0.01$ events/(s $\times$ Bq) for the NaI, $N = 2.97 \pm 0.06$ events/s and $E = 0.0101 \pm 0.0002$ events/(s $\times$ Bq) for the HPGe.

In the end, we can conclude that the radon activity per liter of air in the room at the Polo didattico building is RN = 2.36 $\pm$ 0.26 Bq/L for the NaI and RN = 1.68 $\pm$ 0.18 Bq/L for the HPGe, pretty high values.

We can also calculate the RN factor using directly the value of the activity computed with our method; using data from table 1.9 we can write

$$\mathrm{RN} = \frac{A}{\mathrm{DF} \times \mathrm{CF} \times t} \ ,$$

where A is the activity (in Bq) in the region of interest. With this, we obtained RN = 3.22 $\pm$ 0.34 Bq/L for the NaI and RN = 4.77 $\pm$ 0.38 Bq/L for the HPGe, and we immediately notice the discrepancy between the other two RN values.

At last, we measured an autunite sample activity. The procedure for this measure is the same we used in the measure of the pellet and plaster activities and the results are resumed in figure 1.14 and table 1.12.

1.2 Conclusions

On the measures of the activities we encountered a systematic discrepancy between the measures of the NaI detector and the HPGe detector; this can be due to an overes-

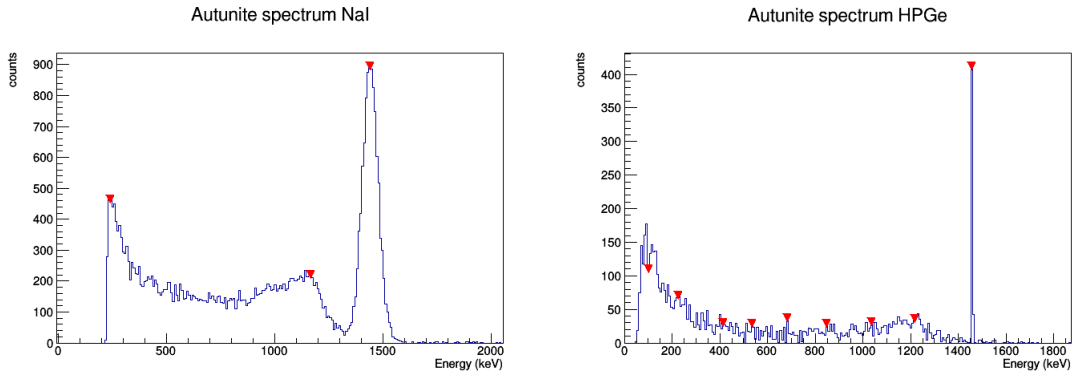

Figure 1.14: Source spectrum of autunite and relative peaks.

Autunite analysis
Measurement time: 1120 s
Weight: 0.029 kg

NaI detector					
Peak (keV)	Counts	Efficiency	Activity (Bq/kg)	Percent	Radionuclide
241	8600 ± 92	0.530 ± 0.021	2671.20 ± 30.34	0.14	^{132}Te
1166	8427 ± 91	0.240 ± 0.010	5772.24 ± 66.16	0.31	^{207}Bi
1438	10330 ± 101	0.168 ± 0.007	10137.06 ± 106.07	0.55	^{40}K

Total activity with NaI: 18580.49 ± 202.56 Bq/kg

HPGe detector					
Peak (keV)	Counts	Efficiency	Activity (Bq/kg)	Percent	Radionuclide
100	1844 ± 42	0.585 ± 0.070	5298.12 ± 124.81	0.07	^{155}Eu
228	858 ± 29	0.449 ± 0.054	3212.87 ± 110.28	0.04	^{132}Te
415	489 ± 22	0.305 ± 0.037	2696.42 ± 122.31	0.04	^{198}Au
534	325 ± 18	0.238 ± 0.029	2292.54 ± 127.43	0.03	^{115}Cd
684	205 ± 14	0.175 ± 0.021	1972.44 ± 137.94	0.03	^{187}W
850	392 ± 19	0.124 ± 0.015	5317.87 ± 269.26	0.07	^{131}Te
1037	407 ± 20	0.084 ± 0.010	8130.51 ± 404.05	0.11	^{207}Bi
1216	796 ± 28	0.058 ± 0.007	23031.34 ± 820.44	0.30	^{91}Y
1456	518 ± 22	0.035 ± 0.004	24628.89 ± 1085.68	0.32	^{40}K

Total activity with HPGe: 76581.01 ± 3202.21 Bq/kg

Table 1.12: Data elaboration for the measure of the activity of the autunite sample.

timation of the efficiencies of the NaI and HPGe detectors as we have already pointed out. All the sources are taken to emit isotropically and to be point like, and the apparatus was supposed to be perfectly aligned, these could be possible sources of errors in the computation of the solid angle, and the great majority of the measurements of the whole experiment depend crucially on the solid angle measurement (efficiencies, activities...). In general all the activity measurements are pretty high, and this is confirmed also on the comparison between the RN values, in fact the ones obtained with the reference canister help are lower than the ones obtained directly with the exposed canister. Also again we notice that the HPGe overestimates the activity, a systematic error almost certainly due to wrong solid angles computations and an overestimation of the peaks detected. Further analysis could try to consider only peaks whose FWHM is not less than the calculated resolution of the relative detector.

If we consider as good data the RN measures with the help of the reference canister, we should conclude that the room at Polo didattico building is not too much safe when considering radon radioactivity, but one can notice how the values of the two detectors, even if they are close, are incompatible.

In the end we must unfortunately conclude that we didn't manage to properly reach the goals of this experiment.

2 Compton scattering

The objectives of this experiment are:

1. To verify the relationship between energy and angle of the scattered photon;
2. To measure the differential cross section of Compton scattering.

The apparatus consists in a ^{22}Na source that is collimated using a properly shaped lead brick in order to obtain a photon beam with a properly defined geometry. The beam hits the SCATTERER which, for the first part of the experience, consists of a NaI(Tl) scintillator detector mounted vertically. The NaI(Tl) scintillator used as scatterer is a cylinder with diameter 7.5 cm and height 7.5 cm. As the ^{22}Na source yields gamma of 511 and 1275 keV, the photons that hit the Scatterer have to be selected. To this purpose the incoming beam can be "tagged" using the coincidence with a second 511 keV photon that is emitted by the source. To detect the "tagging" photon a second NaI(Tl) scintillator similar to the first is used. Such detector is named TAGGER. The coincidence between the TAGGER and the SCATTERER provide the trigger for the scattered event and can be used to normalize the measurements. The scattered photons are detected at an angle θ_{lab} by a third NaI(Tl) scintillator (like the first two), named DETECTOR. Such scintillator is placed on a rotating arm that allow the variation of the angle θ_{lab}.

2.1 Experiment and data analysis

2.1.1 Calibration

On the graphs showed in figures 2.1-2.7 and table 2.1 we resume the calibration procedure, done with a ^{22}Na source. All the errors relative to count measures reported in this and in the following sections are taken as the square root of the number of counts.

In table 2.2 we verified the relationship between statistics in gamma spectrum and measurement accuracy. In order to do that, we performed a gaussian fit for the 511

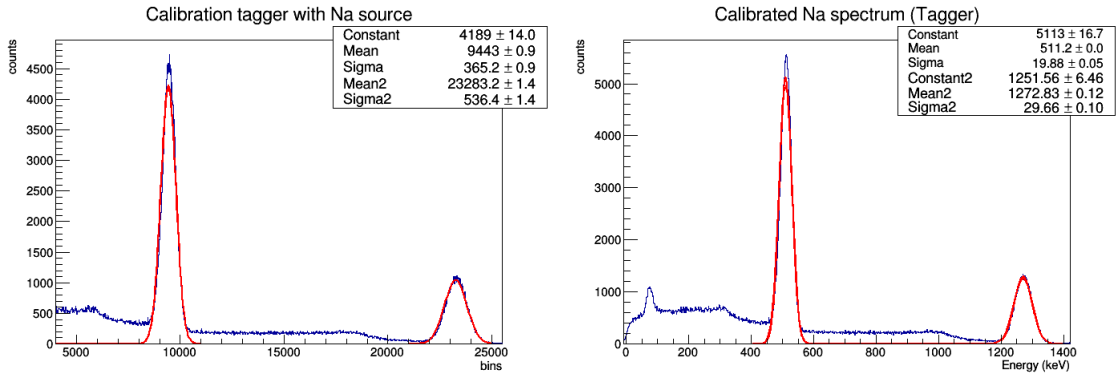

Figure 2.1: ^{22}Na source spectrum for the two peaks for calibration of the tagger.

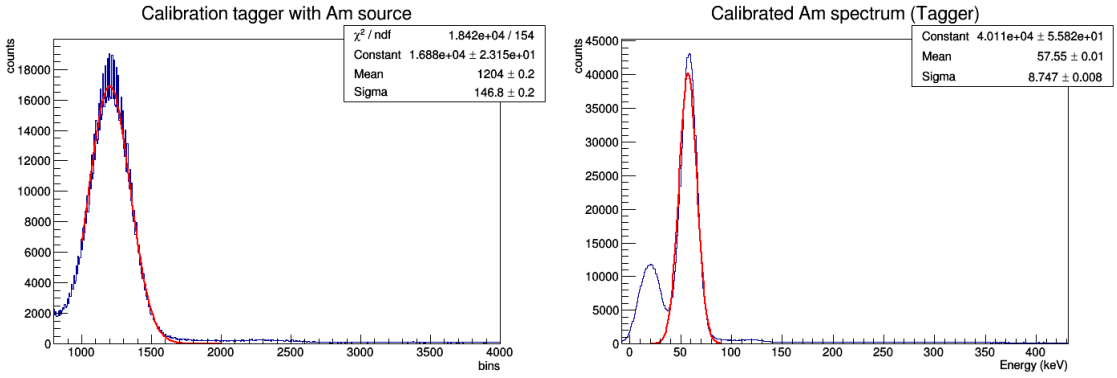

Figure 2.2: ^{241}Am source spectrum of the peak for calibration of the tagger.

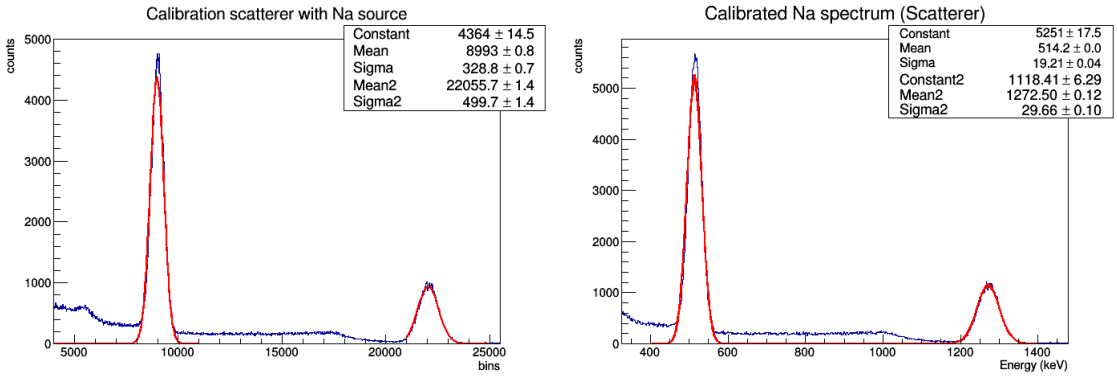

Figure 2.3: ^{22}Na source spectrum of the peaks for calibration of the scatterer.

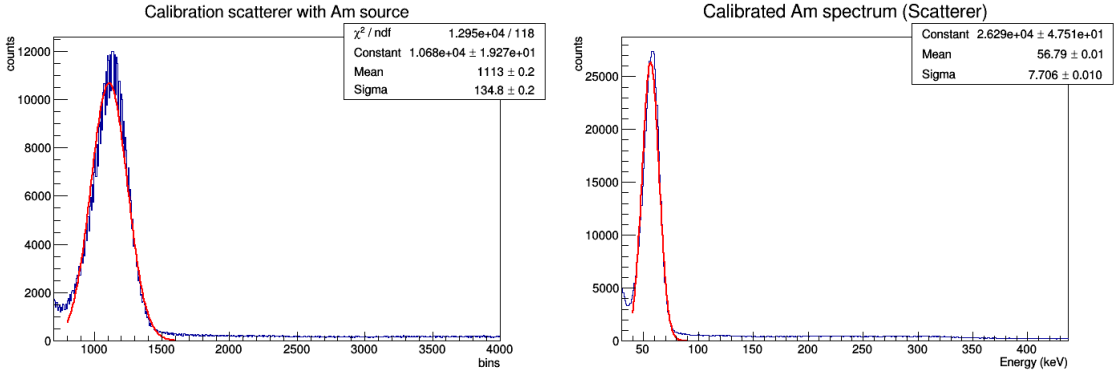

Figure 2.4: ^{241}Am source spectrum of the peak for calibration of the scatterer.

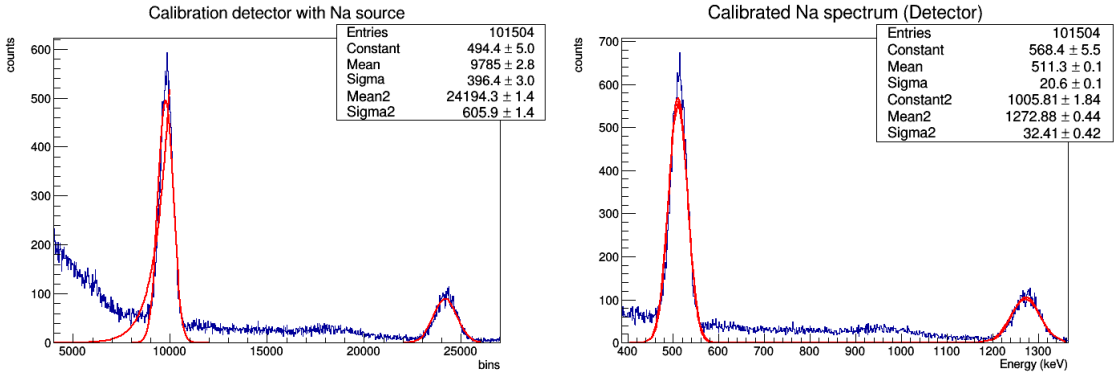

Figure 2.5: ^{22}Na source spectrum of the peak for calibration of the detector.

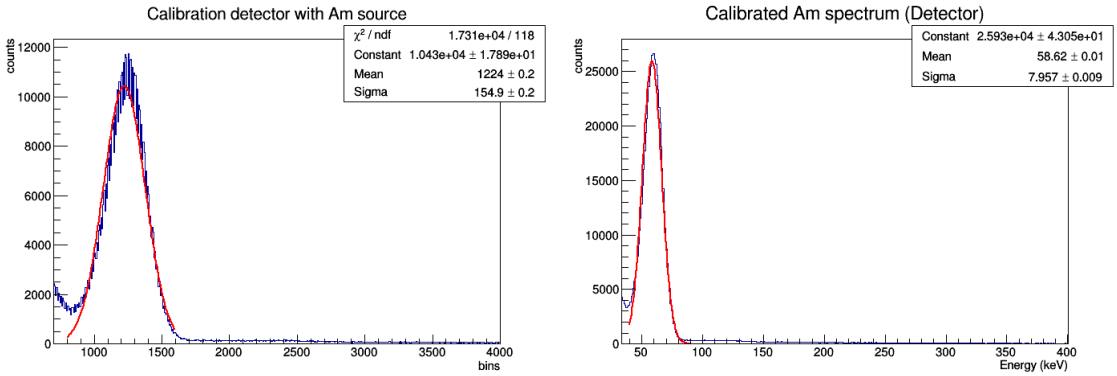

Figure 2.6: ^{241}Am source spectrum for calibration of the detector.

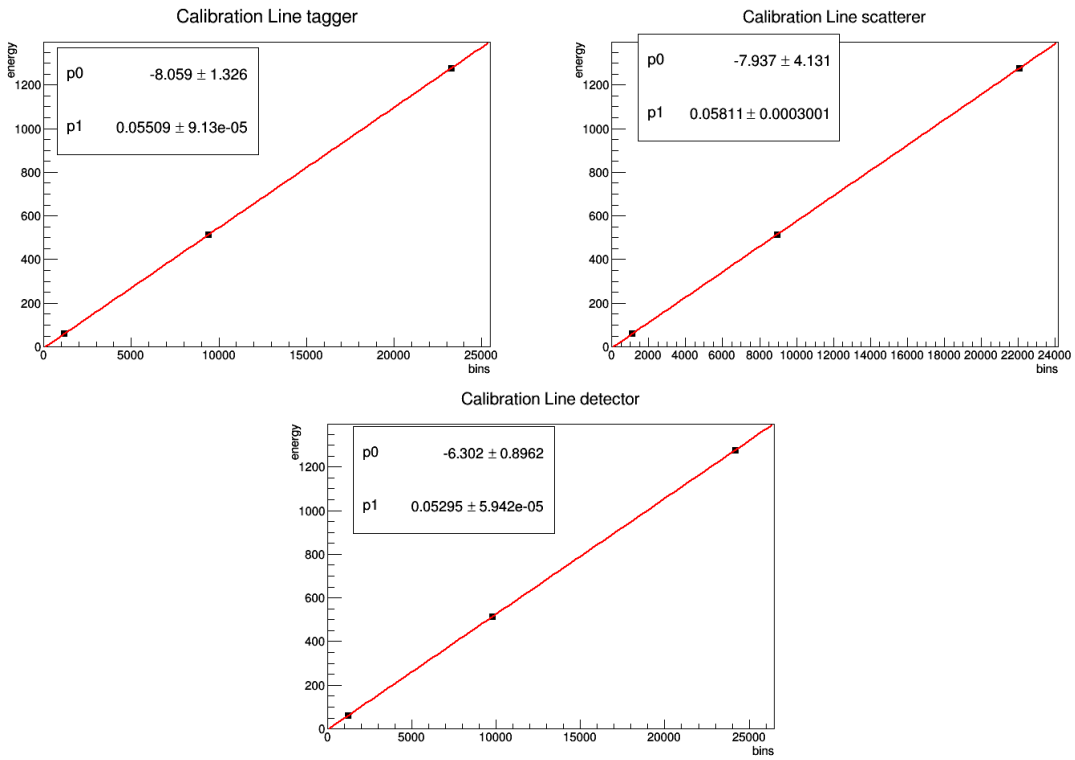

Figure 2.7: Calibration lines for the three detectors.

Peak (keV)	Resolution		
	Tagger	Scatterer	Detector
59	0.356	0.317	0.319
511	0.092	0.088	0.095
1275	0.055	0.055	0.059

Detector	energy calibration (keV)	
	m	q
Tagger	0.0551 ± 0.0001	-8.059 ± 1.326
Scatterer	0.05811 ± 0.0003	-7.937 ± 4.131
Detector	0.05295 ± 0.00005	-6.302 ± 0.896

Table 2.1: Resume of the calibration of the detectors.

Entries	Centroid error
3840	25.01
11584	8.16
51135	3.84
101504	2.74

Table 2.2: Resume of the analysis on the relation between statistics in gamma spectrum and measurement accuracy in the detector.

keV peak for various spectra obtained with different number of entries, and reported the centroid values and their error.

For the sodium spectrum of the tagger, we can determine the fraction of events due to 511 keV photons. We can define the ratio F(511) as

$$\mathrm{F}(511) = \frac{\mathrm{A}(511)}{\mathrm{A}_t} \ , \tag{3}$$

where A(511) is the area below the first sodium peak and A_t is the total area of the spectrum (each of the two areas is calculated subtracting the background). In our experiment, we obtained $\mathrm{A}_t = (5.254 \pm 0.007) \times 10^5$ and $\mathrm{A}(511) = (1.586 \pm 0.004) \times 10^5$ so F(511)=0.302 ±0.001. This result will be used to calculate the cross section.

2.2 Study of the scattered photon

The scattered photon and the scattered electron involved in Compton scattering should obey the following relations regarding their energy:

- for the scattered photon, using the well known result regarding the wavelengths of initial photon and final photon and the De Broglie relation $E = \frac{hc}{\lambda}$, we should

reproduce

$$E_f^\gamma = \frac{E_i^\gamma}{1 + \frac{E_i^\gamma}{m_e c^2}(1 - \cos\theta)} \ ,$$

where θ is the scattered angle, E_f^γ the energy of the outgoing photon, E_i^γ the energy of the incoming photon and m_e the mass of the electron;

- assuming for the electron to be at rest in our laboratory frame, by conservation of energy we should also be able to reproduce

$$E_f^e = E_i^\gamma - E_f^\gamma \ ,$$

with obvious notation.

In table 2.4 are reported the measured number of photons and of electrons. All the measures in this section are taken using the triple coincidence between the three detectors; we considered as acceptable a photon energy event detected in the tagger if its energy was in the range $E_m - 2\sigma < E < E_m + 2\sigma$, where E_m is the centroid value of the fitting gaussian for the peak of interest and σ^2 is its variance, whereas we considered as acceptable an electron energy that is less than $E_m^s + 2\sigma_s$ (same notation as before but referred to the scatterer), this in order to avoid events that are not caused by the 511 keV photons.

In table 2.3 we resume the analysis on the energy of the electron and of the photon whereas in figure 2.8 we illustrate the comparison between our values and the theoretical ones; the energies reported are the average energies revealed in the full-energy peak. In figure 2.9 we illustrate the sum of the energy revealed in the scatterer and in the detector event by event in such a way that one can verify the energy conservation from the spectrum, whereas in figure 2.11 we show the two dimensional energy spectrum of scatterer and detector (to make the correlation between the points more evident we have put only events that satisfies the energy conservation, i.e. we accepted an event if $E_t - \sigma_t < E < E_t + \sigma_t$, where E is the sum of the energies of detector and of scatterer of a particular event, E_t is the sum of the centroid values of interest of the full spectra of detector and scatterer and sigma the associated error).

Just for comparison, we also show in figure 2.10 an example of a bidimensional histogram without the gate on conservation of energy and on the electron energy on the scatterer; we can notice some points below the straight line of the conservation of energy and on the 511 keV line for the scatterer, this last one corresponding probably to photons that have lost all the energy on the scatterer without making the scattering with any electron (the coincidence between these photons and the event in the detector is probably due to the background and noise).

The data for the 90 degrees measurement have an high statistic since it refer to a measurement time of almost 20 hours.

Angle	E_γ (th.) (keV)	E_e (th.) (keV)	E_γ (keV)	E_e (keV)	$E_\gamma + E_e$ (keV)
0	511.00	0.00	483.00 ± 35.47	23.48 ± 19.78	506.48 ± 55.25
30	453.31	57.69	436.10 ± 53.94	66.70 ± 36.30	502.80 ± 90.24
50	381.34	129.66	370.30 ± 62.46	128.40 ± 53.38	498.70 ± 115.84
90	260.82	250.18	274.90 ± 44.25	233.70 ± 49.52	508.60 ± 93.77

Table 2.3: Resume of the analysis on the energy measured of the photon and of the electron (compared with the theoretical values indicated with (th.)).

Angle	N_γ	N_e
0	2796 ± 52.88	2202 ± 46.93
30	3501 ± 59.17	3937 ± 62.75
50	4195 ± 64.77	5229 ± 72.31
90	144800 ± 380.53	188200 ± 433.82

Table 2.4: Resume of the analysis on the measured number of photons and of electrons.

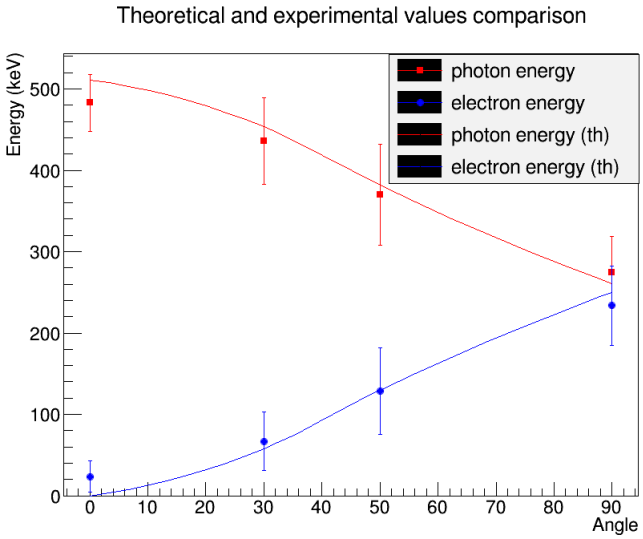

Figure 2.8: Graphics of the energy of the photon and of the electron compared to the theoretical values.

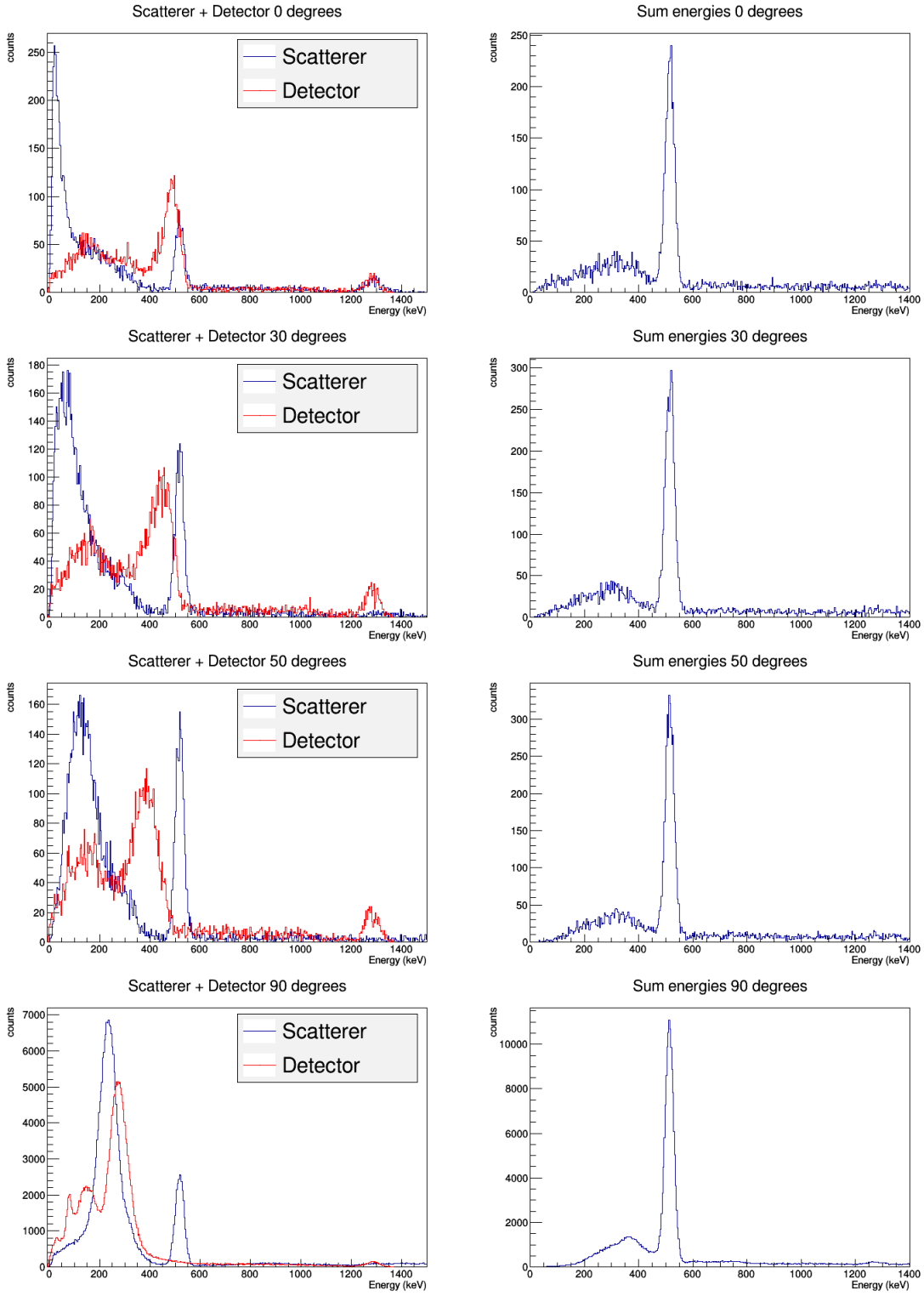

Figure 2.9: Graphics showing the sum of the energies event by event.

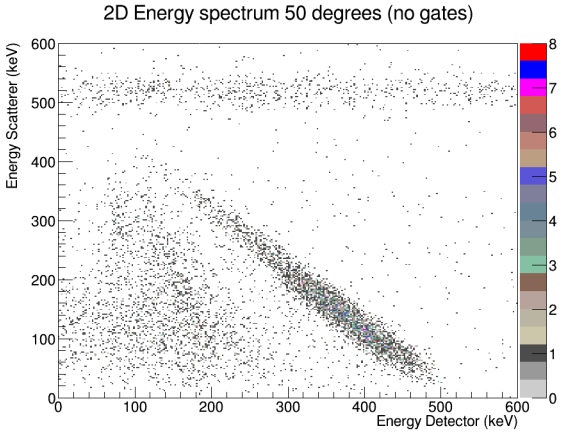

Figure 2.10: Two dimensional histograms of the energy spectrum scatterer-detector for 50 degrees without the gate on conservation of energy and on the electron energy on the scatterer.

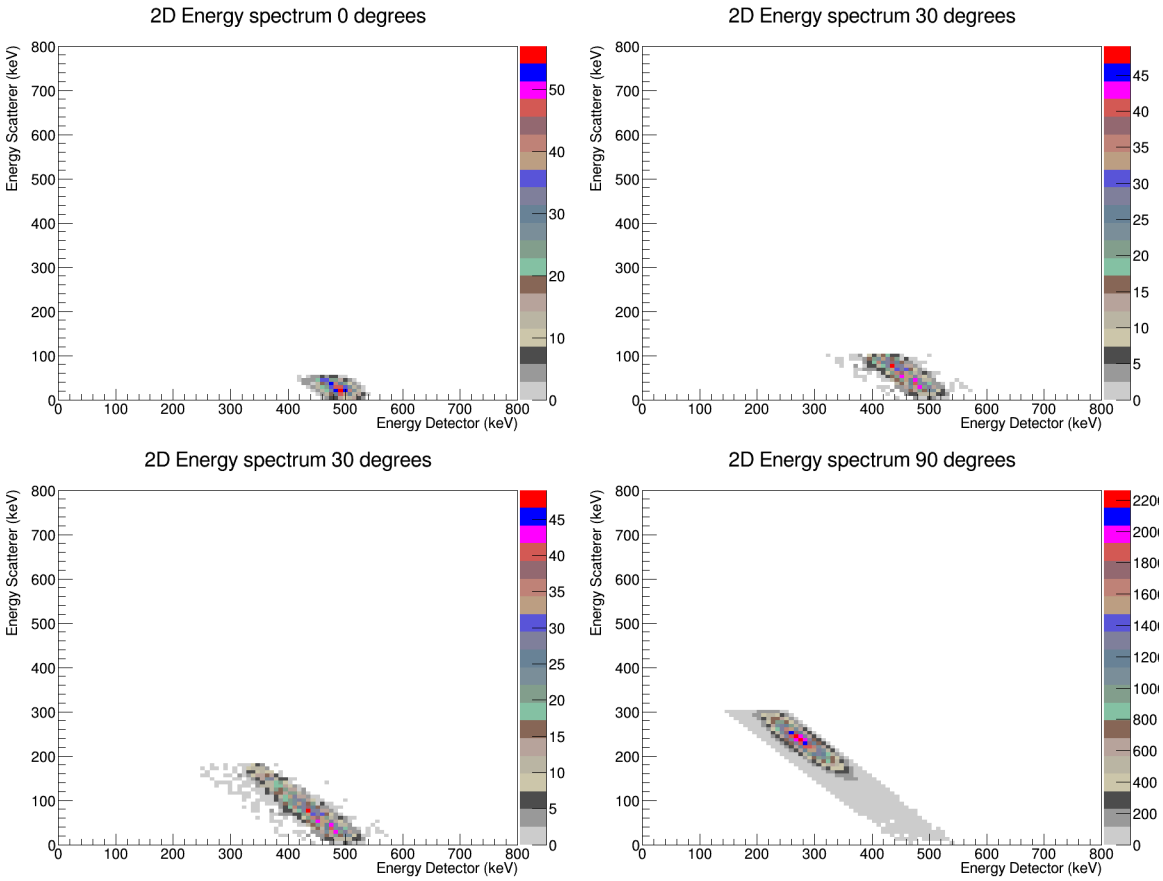

Figure 2.11: Two dimensional histograms of the energy spectrum scatterer-detector.

2.3 Measurement of the Compton cross section

In this part of the experiment we want to obtain the cross section of an aluminium sample. The formula for the measure of the experimental Compton scattering is:

$$\left.\frac{\mathrm{d}\sigma}{\mathrm{d}\Omega}\right|_{\mathrm{exp}} = \frac{\Sigma_\gamma}{\epsilon \times N \times \Delta\Omega_f \times \frac{I}{S}} \ ,$$

where Σ_γ is the number of events in the full energy peak of the scattered photon, ϵ is the efficiency for the energy of the scattered photons, N is the number of electrons in the sample of aluminium, $\Delta\Omega_f$ is the solid angle underlined by the detector and $\frac{I}{S}$ the number of accidental photons hitting the sample per unit surface.

To obtain N, it suffices to use the following formula:

$$N = \frac{V \rho_{\mathrm{Al}} N_a Z}{m_a} \ ,$$

where $V = 9.05 \pm 0.12$ cm^3 is the volume of the sample, $\rho_{\mathrm{Al}} = 2.7$ g/cm^3 is the density of the aluminium, $Z = 13$ is the atomic number, N_a is the Avogadro number and $m_a = 27$ g/mol is the atomic weight. In the end $N = (4.97 \pm 0.71) \times 10^{24}$.

For Ω, we used (2) and found $\Omega = 0.089 \pm 0.008$ (since the distance from the detector we used was $d = 22.0 \pm 0.2$ cm);

To obtain ϵ, we used the spectrum obtained by putting the detector at zero degrees and in contact with the source lead collimator and using as the master gate the coincidence between the tagger and the detector to obtain the total number N_t of events in the spectrum of the tagger and the number N_d of events in the 511 keV peak of the detector. Then, since in our measure $N_d = (5.149 \pm 0.007) \times 10^5$ and $N_t = (7.549 \pm 0.009) \times 10^5$,

$$\epsilon(511\mathrm{keV}) = \frac{N_d}{N_t} = 0.682 \pm 0.001 \ .$$

The measure of Σ_γ is obtained placing the detector at an angle of 90 degrees. The resulting spectrum is taken using the coincidence between the tagger and the detector, and we found $\Sigma_\gamma = 2630 \pm 51$ (showed in figure 2.12).

The last quantity we need is I; to compute it, we can use $I = N_{scaler} \times \mathrm{F}(511)$, where F(511) is reported in (3) and N_{scaler} is the number of events in the tagger without the coincidence condition. So I is the number of 511 keV photons that hit the tagger and were processed by the electronics. We found $I = (3.277 \pm 0.015) \times 10^7$.
In the end we obtained for the cross section

$$\left.\frac{\mathrm{d}\sigma}{\mathrm{d}\Omega}\right|_{\mathrm{exp}} = (1.17 \pm 0.08) \times 10^{-26} \ \mathrm{cm}^2 \ ,$$

whereas the theoretical value of the cross section for the aluminium computed at 90 degrees, using the following (Klein-Nishina formula)

$$\frac{\mathrm{d}\sigma}{\mathrm{d}\Omega} = \frac{r_e^2}{2}\left(\frac{E_f^\gamma}{E_i^\gamma}\right)^2 \left(\frac{E_f^\gamma}{E_i^\gamma} + \frac{E_i^\gamma}{E_f^\gamma} - \sin^2\theta\right) \ ,$$

is $\mathrm{d}\sigma/\mathrm{d}\Omega = 1.505 \times 10^{-26}$ cm^2.

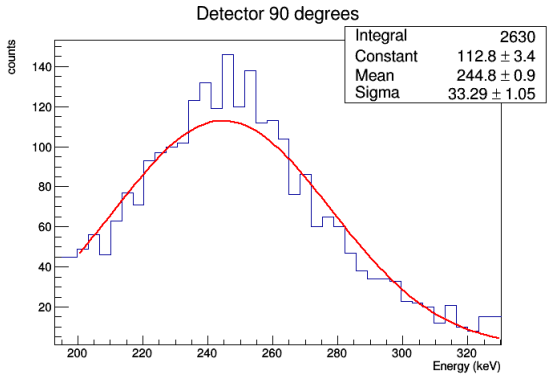

Figure 2.12: Spectrum for the measure of Σ_γ; notice the peak is near 250 keV as expected for a 90 degrees measurement.

2.4 Conclusions

We managed to reproduce the relation between energy of the scattered electron and the energy of the scattered photon, and we also verified the conservation of the energy. We must remark however that, as one can see from table 2.3, the errors are a bit large, since they are taken as the standard deviation of the gaussian fit of the relative peaks.

Regarding the measure of the Compton cross section for the sample of aluminium at 90 degrees, we obtained a value that is close but not compatible to the theoretical one, maybe because of the efficiency of the detectors that misses some events and underestimate the number of counts in the photopeak.

3 Digital Imaging

The objectives of this experiment are:

1. To measure the mass attenuation coefficient for 511 keV photons in different materials;
2. Build a digital image of an unknown sample inside a black-box and determined the material of the object.

Regarding the experimental setup, a ^{22}Na source is placed into an iron collimator with a diameter of 3 cm to obtain a photon beam with a defined collinear geometry. The first gamma detector is placed on one side of the collimator (D#1) to detect one of the two collinear 511 keV photons from the annihilation of the positronium emitted by the ^{22}Na source. A vertical linear array of 7 gamma detectors is placed in the opposite direction (D#2,...,D#8). A computer-controlled slide equipped with a step-by-step engine allows the positioning of the samples in front of the linear array of detectors at predefined position. Detector D#1 is used as tag detector in the experiment. All the measurements are taken in coincidence using for the trigger the following logical condition: D#1. AND (D#2.OR. D#3.OR. D#4.OR. D#5.OR. D#6.OR. D#7.OR. D#8).

3.1 Experiment and data analysis

3.1.1 Calibration

In order to properly calibrate the detectors, we used a ^{22}Na source. The calibration procedure goes the same way as in the previous two experiments, so we show in detail the calibration for the detector 1 only in figure 3.1 whereas we resume the calibration for all the detectors in table 3.1.

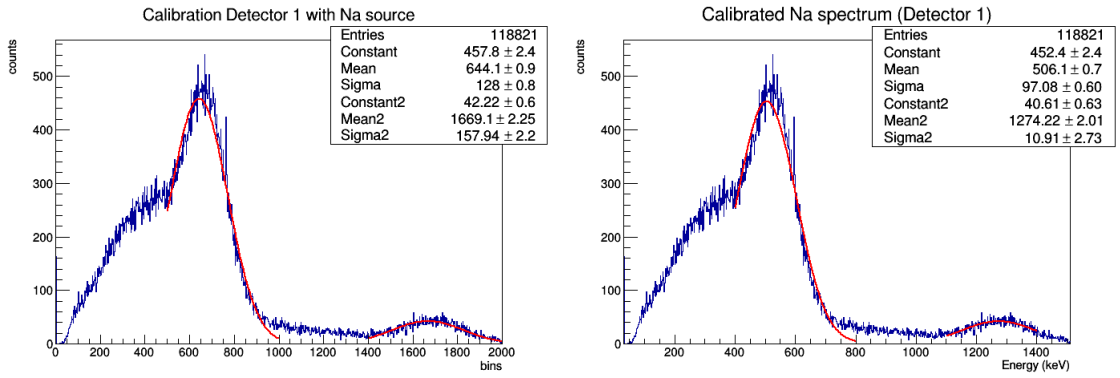

Figure 3.1: ^{22}Na source spectrum for the two peaks for calibration of the first detector.

Detector	m	q	Resol (511 keV)	Resol (1275 keV)
Detector 1	0.745 ± 0.001	30.96 ± 1.75	0.44	0.25
Detector 2	0.996 ± 0.002	-57.84 ± 2.30	0.38	0.25
Detector 3	1.849 ± 0.003	-0.83 ± 1.78	0.38	0.30
Detector 4	1.396 ± 0.003	0.77 ± 1.82	0.40	0.22
Detector 5	1.154 ± 0.002	6.95 ± 1.79	0.43	0.23
Detector 6	1.086 ± 0.002	29.41 ± 1.75	0.41	0.23
Detector 7	1.186 ± 0.002	-86.54 ± 1.91	0.46	0.32
Detector 8	1.086 ± 0.002	-12.42 ± 1.81	0.44	0.25

Table 3.1: Resume of the calibration and the resolution measurements of the 8 detectors.

Material	Thickness (mm)	μ/ρ (10^{-2} cm^2/g)	Density (g/cm^3)
Aluminium	20	8.44	2.69
Lead	5	16.14	11.35
Polyethylene	20	9.95	0.93
Iron	10	8.41	7.87
Graphite	20	8.71	1.70

Table 3.2: Data of the sample used, the experimental values for the attenuation coefficient are taken from `https://physics.nist.gov/PhysRefData/XrayMassCoef/tab3.html` (notice that these data are from the 0.5 Mev row roughly corresponding to the energy of the 511 kev photon).

3.1.2 Attenuation Measurements

In this section we exploit the fact that for the intensity of the electromagnetic radiation, when it crosses a certain material, the following equation holds:

$$I = I_0 e^{-\mu_{\text{mass}}\rho x}, \quad \mu_{\text{mass}} = \frac{\mu}{\rho} \ ,$$

where I and I_0 represent respectively the number of photons in a fixed energy range with and without the sample; μ_{mass} represents the mass attenuation coefficient and it is function of the energy of the photon and the atomic number of the material; ρ is the density of the material and x is its thickness. Due to this, we can measure the attenuation coefficients and compare them with the results present in the literature. In order to do that, we measure the attenuations I/I_0 using the spectrum of the pattern unit and we compare them with the one calculated using data from table 3.2. All the spectra presented in this section are obtained with a 15 minutes measurements. All the data written in this and in the following section refer to the events that have released an energy E in the detector 1 such that $E_m - 2\sigma < E < E_m + 2\sigma$, where E_m is the centroid value of the fitting gaussian for the peak at 511 keV and σ^2 is its variance. This in order to exclude the 1275 keV photons from the analysis.

Since the position of the detectors affects the effective thickness seen by the radiation, we must correct the thickness data by inserting a corrective factor calculated with the

Detector	Angle	Corrective factor
#2	11°	1.019
#3	7°	1.008
#4	4°	1.002
#5	0°	1.000
#6	4°	1.002
#7	7°	1.008
#8	11°	1.019

Table 3.3: Corrective factors due to the fact that the thickness of the material seen by the radiation depends on the position of the detectors.

following:

$$c = \frac{l}{\cos\theta} \ ,$$

where c is the corrective factor, l is the real horizontal width of the sample and θ is the angle measured using $\theta = \arctan(h/d)$, where d is the distance between the source and the array and h is the vertical distance between source and the detector. Results of this procedure are resumed in table 3.3.

In table 3.4 and 3.5 we resume the computation of our experimental attenuation coefficient. As one can easily see, unfortunately we don't have data from detector 3,7,8 due to various problems with the electronics, whereas detector 2 doesn't seem to work properly, it greatly underestimates the number of counts and gives results that are meaningless (for example a negative absorption coefficient for the polyethylene). In the following we will show nevertheless the results associated to detector 2 for completeness but we won't consider it in further analysis.

We notice that the measured absorption coefficients for lead and iron are nearly compatible with respect to the experimental ones, and detector 4 seems to give the closest values; for graphite, we notice a greater mismatch for detector 5 and 6, whereas again detector 4 seems to give the best answer. For aluminium we have a slight discrepancy also for detector 4.

The discrepancies can be due to underestimated errors (we counted only the statistical one, i.e. the square root of counts) and on a non proper setting of the threshold, in particular for detector 5 and 6 (notice that they both always overestimate the experimental values).

For the polyethylene we notice instead that our measured data are very far from the experimental one. This could be due to the fact that a lot of photons are lost in the process due to Compton effect, that is larger on the polyethylene with respect to the other materials. But since we don't have further informations about this issue, we will assume an "effective" attenuation coefficient for the polyethylene corresponding to the one resulting from detector 4, which seems to be the most reliable.

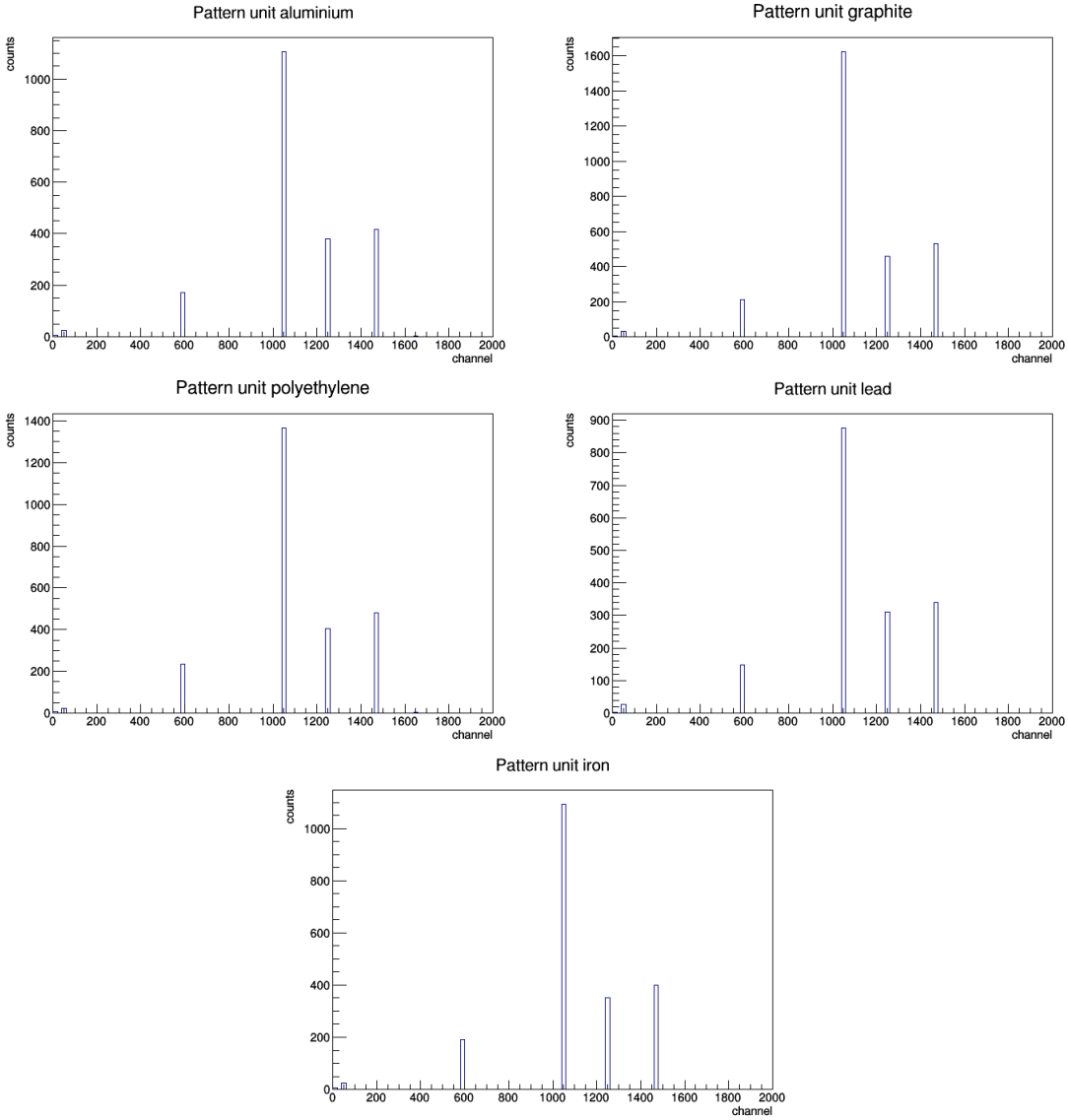

Figure 3.2: Some examples of pattern unit spectra.

Detector	Aluminium	Lead	Polyethylene	Iron	Graphite
2	0.82 ± 0.09	0.71 ± 0.08	1.12 ± 0.11	0.90 ± 0.09	1.00 ± 0.10
3	-	-	-	-	-
4	0.53 ± 0.02	0.42 ± 0.02	0.64 ± 0.02	0.52 ± 0.02	0.78 ± 0.03
5	0.52 ± 0.04	0.43 ± 0.04	0.56 ± 0.04	0.48 ± 0.04	0.63 ± 0.04
6	0.48 ± 0.04	0.39 ± 0.03	0.55 ± 0.04	0.46 ± 0.04	0.61 ± 0.04
7	-	-	-	-	-
8	-	-	-	-	-

Table 3.4: Measure of I/I_0.

Detector	Aluminium	Lead	Polyethylene	Iron	Graphite
2	0.04 ± 0.02	0.06 ± 0.02	-0.06 ± 0.05	0.01 ± 0.01	0.00 ± 0.03
3	-	-	-	-	-
4	0.12 ± 0.01	0.15 ± 0.01	0.24 ± 0.02	0.08 ± 0.01	0.07 ± 0.01
5	0.12 ± 0.01	0.15 ± 0.02	0.32 ± 0.04	0.09 ± 0.01	0.13 ± 0.02
6	0.14 ± 0.01	0.17 ± 0.02	0.32 ± 0.04	0.10 ± 0.01	0.15 ± 0.02
7	-	-	-	-	-
8	-	-	-	-	-

Table 3.5: Measure of the experimental attenuation coefficient (in cm^2/g).

Detector	Position 1	Position 2	Position 3	Position 4	Position 5
2	1.33 ± 0.13	1.39 ± 0.13	1.01 ± 0.10	1.11 ± 0.11	1.10 ± 0.11
3	-	-	-	-	-
4	0.37 ± 0.02	0.35 ± 0.02	0.85 ± 0.03	0.90 ± 0.03	0.85 ± 0.03
5	0.33 ± 0.04	0.29 ± 0.04	0.71 ± 0.04	0.84 ± 0.05	0.77 ± 0.04
6	0.30 ± 0.03	0.32 ± 0.03	0.72 ± 0.04	0.78 ± 0.04	0.73 ± 0.04
7	-	-	-	-	-
8	-	-	-	-	-

Table 3.6: Measure of the attenuation for the black box.

3.1.3 Black box analysis

In order to find out what there was on our black box, we analyzed it in five different horizontal positions and we calculated the attenuation relative to all the seven detectors for each position, thus obtaining a 7×5 matrix. The attenuation measurements are resumed in table 3.6, whereas in table 3.7 we tried to characterize the possible material lying in the corresponding position of the black box exploiting the measures of the attenuation coefficient we previously obtained.

We can see that there is a strong attenuation on position 1 and 2 corresponding to the detectors 4,5,6. The weak attenuation present on the other three positions is incompatible with all the previous five materials examined (unless we make the unrealistic hypothesis that their thickness is less than 1 mm) and could be due to the presence of the black box (nevertheless we notice that, if this were the case, we would have $\mu \simeq 0$ for the black box). From the attenuation values we can conclude, by looking at table 3.8, that probably there were a vertical bar on the left made of lead of about 6 mm thickness or made of iron of about 18 mm thickness. In our opinion, since previously we had a 5 mm lead and a 10 mm iron, the most probable material that was present in the black box was lead.

Detector	Position 1	Position 2	Position 3	Position 4	Position 5
# 2	-	-	-	-	-
# 3	-	-	-	-	-
# 4	Lead	Lead	X	X	X
# 5	Lead	Lead	X	X	X
# 6	Lead	Lead	X	X	X
# 7	-	-	-	-	-
# 8	-	-	-	-	-

Table 3.7: Identification, whenever it is possible, of the most probable material present in the corresponding position of the black box (we've used "-" for the detectors that do not work, and "X" to indicate that there should be nothing but the empty black box).

Material	Thickness (cm)
Aluminium	5.33 ± 0.59
Lead	0.66 ± 0.07
Polyethylene	5.39 ± 0.60
Iron	1.82 ± 0.20
Graphite	8.14 ± 0.90

Table 3.8: Possible thicknesses of the material in the black box compatible with an attenuation $I/I_0 \sim 0.3$; for the polyethylene we used the "effective" coefficient we measured with detector 4.

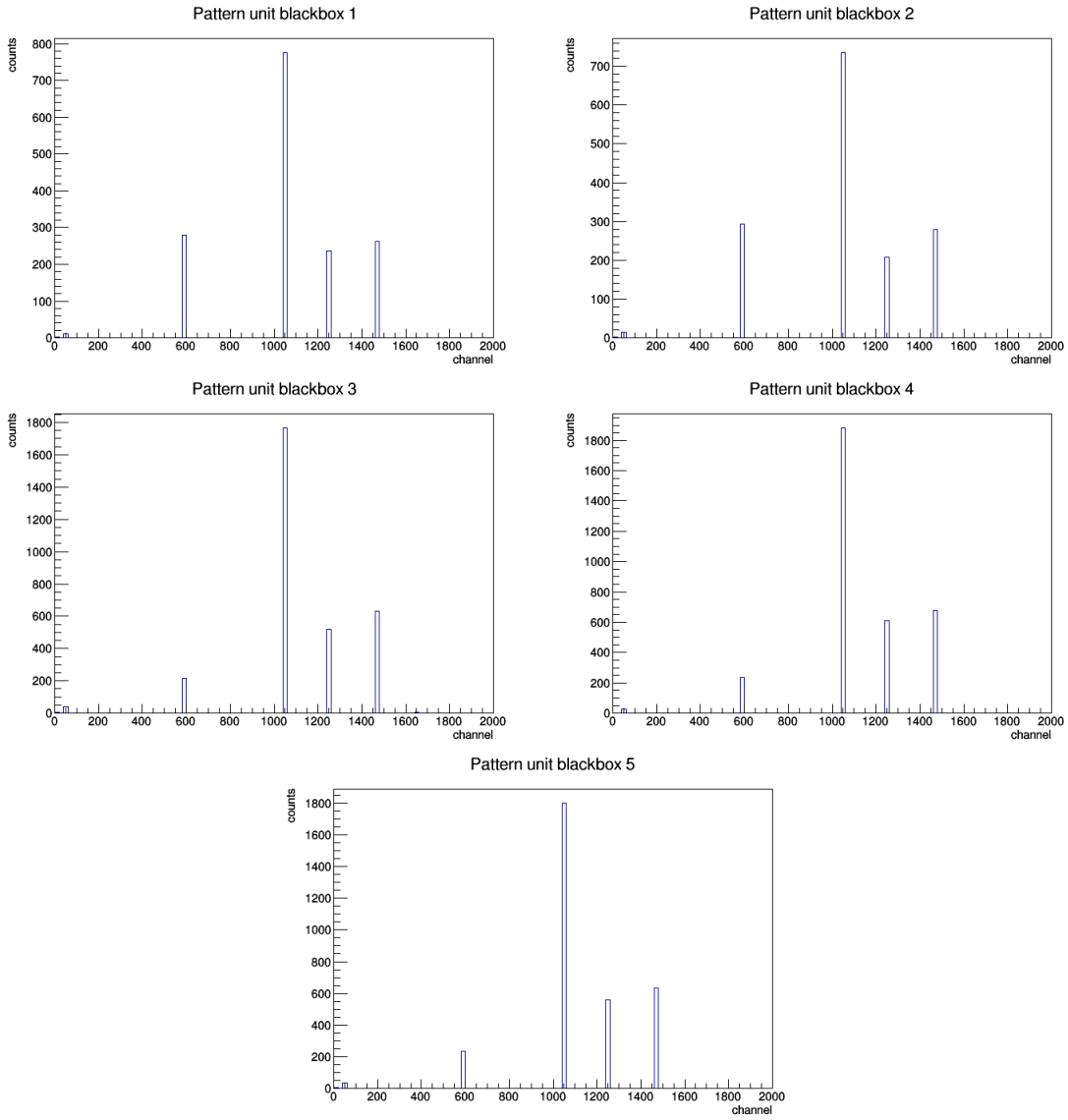

Figure 3.3: Pattern unit of the black box related measurements.

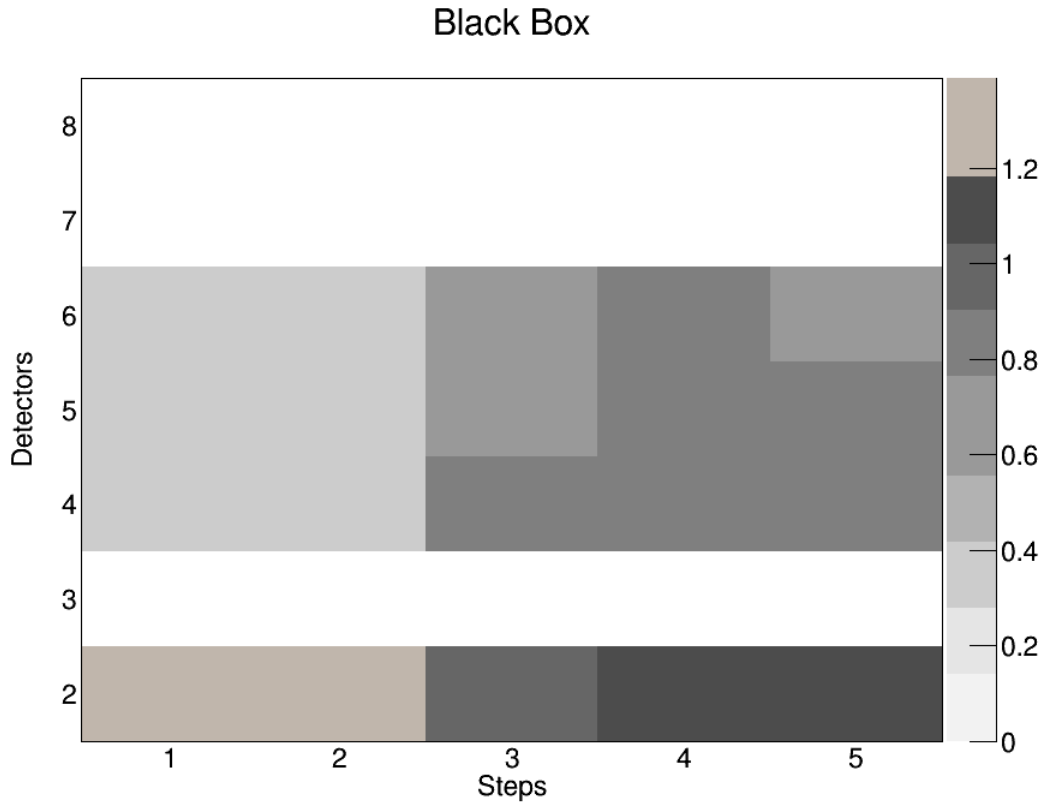

Figure 3.4: 2D representation of the attenuation of the black box. We put the attenuations of detector 3,7,8 at zero.

3.2 Conclusions

To conclude we can say that we almost managed to reproduce the attenuation coefficients present in the literature for the lead, iron, graphite and the aluminium, whereas for the polyethylene our value is pretty far from the experimental one, for reasons we have already pointed out. Regarding the detectors, unfortunately we cannot say much for detector 3,7,8, whereas for detector 2 we suspect that is not working properly due to the very low counts it had (of the order of 200) and due to the inconsistent results we obtained with it, so we didn't consider its measures. The little differences on the measures with the remaining three detectors could be due to the different regulation of the threshold value; in particular detector 4 seems to give the best results.

Finally from our data we can guess that, relatively to the region that in the end we managed to analyze, in the black box there were a vertical bar on the left made of lead with possible thickness of $5 \div 7$ mm.